Brief communication - Vent opening at Campi Flegrei: clues from dyke propagation patterns

Jacopo Selva[1], Nello Mangone[1]

[1] Dipartimento di Scienze della Terra, dell'Ambiente e delle Risorse (DiSTAR), University of Naples Federico II, Naples Italy

Correspondence to: Jacopo Selva (jacopo.selva@unina.it

Abstract. Forecasting future vent opening position is fundamental for managing volcanic hazards, and is usually based on the spatial density of past vents or other crust weakness indicators. Here, a novel empirical approach inspired by dyke propagation models is applied to the Campi Flegrei caldera. Results show that dyke direction correlates with topographic peaks within 6 km from the caldera center, and propagation length exhibits two main peaks at 2 and 4 km, leading to a vent opening probability map with maxima well correlating with recent major seismicity and deformations.

1 Introduction

The Campi Flegrei caldera volcanic activity dates back to the upper Pleistocene, with the oldest volcanic activity estimated at around 80,000 years ago (D'Antonio et al., 2007; Orsi et al. 2009). The first caldera collapse occurred approximately 39,000 years ago with the Campanian Ignimbrite (CI) eruption. The period following the CI is characterised by eruptions confined within the newly formed caldera, both continental and marine. A second major eruption occurred around 14,000 years ago, the Neapolitan Yellow Tuff (NYT), which likely caused a second collapse that shaped the current caldera structure (Sbrana et al., 2021). After the NYT eruption, volcanic activity resumed within the inner caldera (Orsi et al. 2004).

The post-NYT eruptive history is divided into three main epochs. The first epoch comprises a total of 33 eruptions, spaning from 15,000 to 10,600 years ago. The eruptive vents align with the newly formed caldera boundaries, with the most energetic eruption being that of the "Pomici Principali" around 12,300 years ago. The second epoch follows a relatively brief quiescent period and includes nine eruptions dated between 9,600 and 9,200 years ago, primarily concentrated in the northeastern sector of the caldera. The third epoch encompasses a total of 28 eruptions from approximately 5,500 to 3,800 years ago; this epoch is predominantly focused in the northeastern part of the caldera (Agnano area) and secondarily in the northwestern sector (Averno area). The most energetic eruption during this period was that of Agnano-Monte Spina around 4,550 years ago. The long period of quiescence following the third epoch lasted until 1538 AD, when the Monte Nuovo eruption took place in the northwestern sector of the caldera (Di Vito et al., 1999). The caldera has not experienced any eruption since.

28 After NYT, the caldera experienced significant resurgence, accompanied by seismicity, degassing, and slow ground
29 deformation often referred to as bradyseism. The latter is concentrated mainly in the geometrical center of the caldera, in the
30 Pozzuoli area, and major movements were tracked at least from the 4th century AD thanks to the ruins of a Roman temple in
31 the port of this city, known as the Serapeum. The largest known bradyseismic events are the ones related to the last Campi
32 Flegrei eruption (the 1538 Monte Nuovo eruption, Di Vito et al., 1999). In the last century, three main bradyseismic crises
33 occurred in 1950-52, 1970-72, and 1984-86, characterised by episodes of uplift of more than 1 m interrupting a slow
34 long-lasting subsidence (Del Gaudio et al 2010). Approximately in 2005, a slow uplift started, accelerating over time, which
35 now fully recovered the subsidence, exceeding the uplift peaks observed in the last century (Chiodini et al. 2021, Bevilacqua
36 et al. 2024, Giudicepietro et al. 2025). This event is still ongoing.

37 Forecasting vent opening is crucial for any volcanic hazard quantification. Different approaches were adopted at Campi
38 Flegrei through time. Alberico et al. (2002) developed a method identifying crustal weaknesses using geophysical,
39 geological, and geochemical parameters. Their probability map indicated the highest likelihood of vent openings in the
40 central caldera near Pozzuoli. Selva et al. (2012) utilized a Bayesian approach fed by fewer parameters, focusing on tectonic
41 structures to track crust weakness and past vents, shifting the area at higher probability toward the northeastern and
42 northwestern sectors, where post-NYT activity concentrated. Bevilacqua et al. (2015) adopted a method based on Gaussian
43 kernel and accounting for the uncertainty on past vent positions, confirming the northeastern sector (near Agnano and
44 Astroni) as the most likely area for future eruptions. More recently, based on past observations and removing multiple
45 eruptions from clustered vents, Charlton et al. (2018) noted that vent opening occurred substantially randomly within a ring
46 area surrounding the caldera center, corresponding to the NYT ring.

47 Rivalta et al. (2019) studied the physical propagation of magma dikes by modelling the trajectory of potential dikes due to
48 the subsurface stress field and the dike's initial position. Their model accounts for various stresses affecting magma ascent.
49 For calderas, it suggests that eruptive vents are concentrated at specific distances from the centre, influenced by the stress
50 induced by the caldera depression, defining a higher propensity to eruption closer to caldera rims, as noted by Charlton et al.
51 (2020). Considering the caldera depression size, Rivalta et al. (2019) forecasted for Campi Flegrei a potential peak for vent
52 opening at a semiannular belt located between 2.3 and 4.2 km from the caldera center. Rivalta et al. (2019) analyzed also the
53 effect of topographic peaks, which may break the caldera symmetry. They analyzed the case of the Campi Flegrei caldera,
54 explaining the concentration of volcanic activity in the northeastern sector due to the peak of the Camaldoli hill, which
55 creates a stress field favouring magma trajectories in the northeast direction.

56 The main features of Rivalta et al. (2019) model are i) that the geometry of the caldera significantly influences dike
57 propagation outward, promoting eruptions away from the geometric centre a a given distance, and ii) topographic
58 asymmetries create localised stress variations in the subsurface, affecting eruption frequency across different angular sectors.
59 While a sufficiently detailed knowledge of the sub-surface stress state is difficult to reach, it is possible to verify if these two
60 main features left track on the available record of past vent positions, and to use this empirical signature to define new vent
61 opening probability maps.

2 Empirical distribution of direction and length of past dykes

The path of the dykes feeding past eruptions is mainly controlled by the geometry of the caldera, which determines the distance from the centre of the caldera, and by the topographical peaks surrounding the caldera, which establishes preferential directions for propagation. Assuming that the origin at depth of the magma is located at the centre of the caldera, below the location of the maximum observed uplift (Amoruso et al. 2012, Rivalta et al. 2019), past vent positions may track the trajectories of the dykes that fed those eruptions. The centre can be approximately assumed at the point of maximum deformation, representing the centre of the bell-shaped deformation of Campi Flegrei. Here, it is set to LON 4263554 and LAT 451954 (UTM WGS84, zone 33N),

Based on this, it is possible to establish an empirical model for such trajectories by studying the empirical distribution of azimuth (angle to North) and distance-from-the-centre (hereinafter radius) of the caldera of the dykes that alimented past eruptions, and use this model to define a forecast map for future vents. Past vent positions are however affected by significant uncertainty. To account for this, we used the 71 vent positions and corresponding uncertainty bounds defined in Bevilacqua et al. (2015), accounting for the uncertainty by randomly sampling 1000 alternative synthetic positions within the defined uncertainty bounds (Supplementary Figure 1).
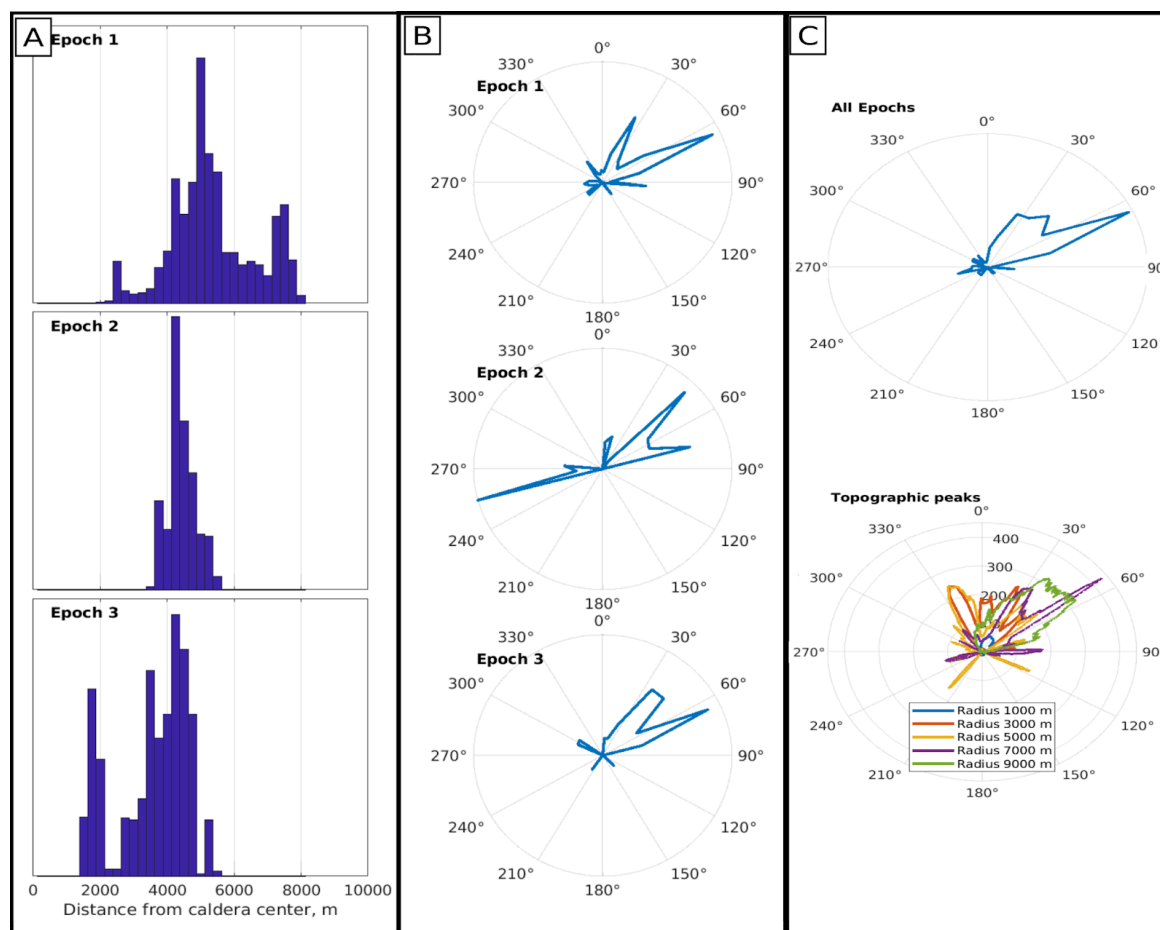
2.1 Length of dyke propagation

At first, we analyse the distances between the centre of the caldera and all post-NYT vents, which represent the length of horizontal propagation of the dykes that alimented such eruptions. The analysis is conducted separately for the three epochs, and jointly for the entire dataset. For simplicity, the recent Monte Nuovo eruption is included in the third epoch. In Figure 1A, we report the empirical distributions (bins of 250 m, the corresponding empirical cumulative distribution functions are reported in Supplementary Figure 2), revealing a strong difference between the first epoch, where 60% of eruptions occur between 4,400 and 6,600 m, and the third epoch that shows shorter distances, with two significant peaks around 4,000 m and 2,000 m, being Epoch 2 somehow intermediate between the other two. A two-sample Kolmogorov-Smirnov test (KS2) confirms that this difference is statistically significant also accounting for vent position uncertainty (significance level of 0.01, Supplementary Figure 3), confirming the already observed progressive inward migration of post-NYT volcanism (Di Vito et al. 1999; Orsi et al. 2004; Isaia et al. 2009; Rivalta et al. 2019).

2.2 Direction of dykes propagation

The direction of propagation of the dykes, which is instead controlled by topographic asymmetries, can be investigated by analyzing the azimuth of the propagation with respect to the centre of the caldera, parameterized as the angle to the North of the line connecting the centre of the caldera and the vent. In Figure 1B, we report the empirical distributions for the different epochs (bins of 20 degrees, the corresponding empirical cumulative distribution functions are reported in Supplementary Figure 2), showing that most of eruptions have an azimuth around 50°, and no specific differences between the distributions

93 are visible. This observation is tested again with a two-sample Kolmogorov-Smirnov test (s.l. 0.01, see Supplementary

94 Figure 3), confirming that the directions of dyke propagation are similar in all epochs, with a primary peak toward NE (50°,

95 toward Astroni, Agnano, and Solfatara).

96

98 **Figure 1: (A) Empirical distribution of distances from the center of the caldera (dyke propagation length) for Epochs 1, 2 and 3.**
99 **(B) Empirical distribution of azimuth (dyke direction) for Epochs 1, 2 and 3. (C) Empirical distribution of azimuth (dyke**
100 **direction) for all Epochs and azimuth of topographic peaks.**

101 Rivalta et al. (2019) suggest that preferential directions may be induced by topographic peaks that modify the stress field. To

102 investigate this empirically, we analyse the maxima of the topography surrounding the caldera, retrieving the maxima in all

103 directions within a given maximum radius. Maximum radii from 2 to 10 km are tested: for each radius, the distribution of

104 topographic maxima as a function of azimuth is normalised and compared with the azimuthal distribution of past eruptions

105 (Figure 1C). For simplicity, the present day topography is adopted, even if some of the edifices (and the corresponding

106 topographic peaks) were built during the post-NYT activity. The comparison confirms the correlation anticipated by Rivalta

107 et al. (2019). The primary peak around 50° corresponds to the topographic peak associated with Starza (for a radius of 1 km)

108 and Camaldoli (for radii of 3 km and larger). In agreement with Rivalta et al. (2019), the latter topographic peak is the most

109 pronounced and it coincides with the highest concentration of eruptive vents during various eruptive periods. A secondary

110 appears in the NNW direction (-45°) for radii larger than 5 km, corresponding to the peak of the Gauro volcanic edifice

111 (Monte Barbaro): this edifice was created during one of the first eruptions of the first epoch, and does not correspond to any

112 peak in the observed distribution of azimuth. Performing a Kolmogorov-Smirnov test between the angular distributions of

113 past vents and of topographic peaks, the largest p-values correspond to a maximum distance of 7 km, which is the only case

114 for which the null hypothesis of equal distribution is consistently not rejected independently from vent position uncertainty

115 (s.l. 0.01, Supplementary Figure 4).

116 **3 Vent opening probability**

117 The empirical distributions obtained in Section 2 can be used to set a vent opening probability map. The probability density

118 function in a specific point in the caldera can be calculated in polar coordinates using the following formula:

119
$$f_{pol}(r, \theta) = f_r(r) f_\theta(\theta). \tag{1}$$

120 where the term $f_\theta(\theta)$ is the angular probability distribution, the term $f_r(r)$ is the probability distribution for the distances

121 from the center of the caldera. In this formulation, it is assumed that these two distributions can be considered independent,

122 being the latter fundamentally controlled by the nearly circular shape of the caldera and the former predominantly controlled

123 by local topographic features. This probability distribution can be transformed into Cartesian coordinates as follows:

124

125
$$f_{xy}(x, y) = \frac{1}{r} f_{pol}(r, \theta) = \frac{1}{r} f_r(r) f_\theta(\theta) \quad . \tag{2}$$

126 where the term $f_{pol}(r, \theta)$ is factorized in its two independent terms.

127 To develop the probability map, we define a grid 14.5 x 12.5 km, centered at LON 427406 and LAT 4518958 (UTM WGS

128 84 33N), with 700 square cells 500 x 500 m, equal to the one adopted in Selva et al. (2012). Then, the probability in each

129 cell can be computed by numerically integrating $f_{xy}(x, y)$ computed through Eq. (2), where the terms $f_r(r)$ and $f_\theta(\theta)$ can

130 be set using the empirical distributions developed in Section 2.

131 In particular, we propose 2 alternative implementations. At first, we consider for both $f_r(r)$ and $f_\theta(\theta)$ the empirical

132 distributions that may be considered representatives of the present state of the caldera. In particular, we set $f_r(r)$ as the radial

133 distribution of the eruptions of Epoch 3 (including also Monte Nuovo), which is indeed the most recent and significantly

134 different from the one of the previous epochs. Then, we set $f_\theta(\theta)$ as the azimuthal distribution of all post-NYT eruptions, as

135 the different epochs are statistically indistinguishable. The result is reported in Figure 2A. A second implementation is also

136 tested by substituting the empirical azimuthal distribution with the distribution of the topographic maxima for a radius of

137 7,000 m, the one that better correlates with past vents. The results are reported in Figure 2B. The numerical values for both

138 models are reported as Supplementary File.
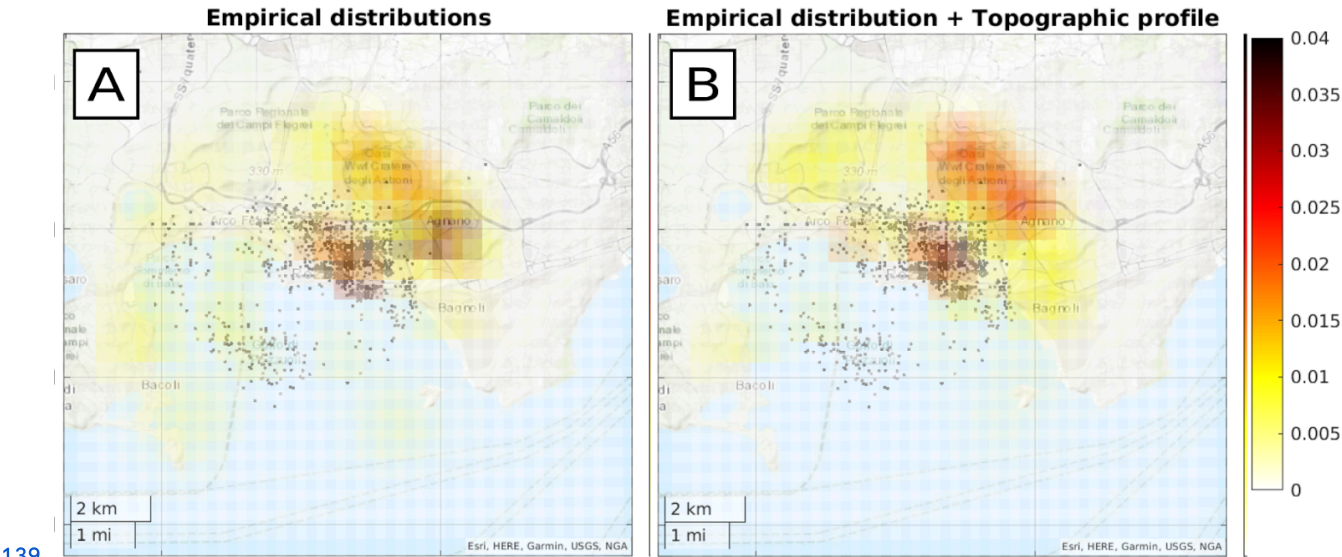
Figure 2: Vent opening probability maps: (A) based empirical distances and azimuth, (B) based on empirical distances and topographic azimuth. Black dots indicate seismicity (Md > 1.0) in the period June 2023 - June 2025.

4 Discussion

143 The two probability maps in Figure 2 are similar, with two distinct probability peaks in the NE direction at about 4 and 2 km

144 from the center, corresponding to the Agnano-Astroni and the Solfatara area, respectively. Considering the topographic

145 contribution (Figure 3B), the angular probability values are more distributed than when the empirical distribution is

146 considered (Figure 3A). The effect is that the maximum probability value in the area at NW is almost halved. The relative

147 peaks in the other directions appear relatively more evident when only empirical distributions are considered, generating two

148 concentric and separated rings at about 2 and 4 km, with secondary peaks also in the submerged side of the caldera toward

149 the E and SE, in the direction of Baia and Bacoli, as well as the inland area toward NNW.

150 Comparing these results with the main probability maps for Campi Flegrei discussed in the literature, interesting

151 coincidences and some significant differences emerge. The map produced by Alberico et al. (2002) differs widely from all

152 others, having maximum values in the center of the caldera and close to 0 in the peripheral areas, which is in contrast with

153 the empirical evidence. The higher probability areas of Selva et al. (2012) and Bevilacqua et al (2015) (Figure 3A-B), such

154 as the Agnano area to the NE of the caldera, coincide with those identified here. The two peaks at distances of 2 and 4 km

155 from the caldera center are in the range forecasted by Rivalta et al. (2019) when adopting only Epoch III data (Figure 3C).

156 All these salient features are indeed present in all studies, as they essentially correspond to the spatial distribution of past

157 vents. However, there are also some significant differences. The propagation distance distribution here produces two distinct

6

158 peaks at 2 and 4 km, more than a continuous distribution in this range, generating two distinct rings at relatively higher
159 probability. In the areas of Nisida and Campo Miseno, the probability values obtained here are relatively lower than in
160 literature studies. The secondary peak identified in the Averno area in Selva et al., (2012) appears only in the map based on
161 topography, but it is significantly shifted eastward, in the direction of the Gauro, due to its topographical peak.

162
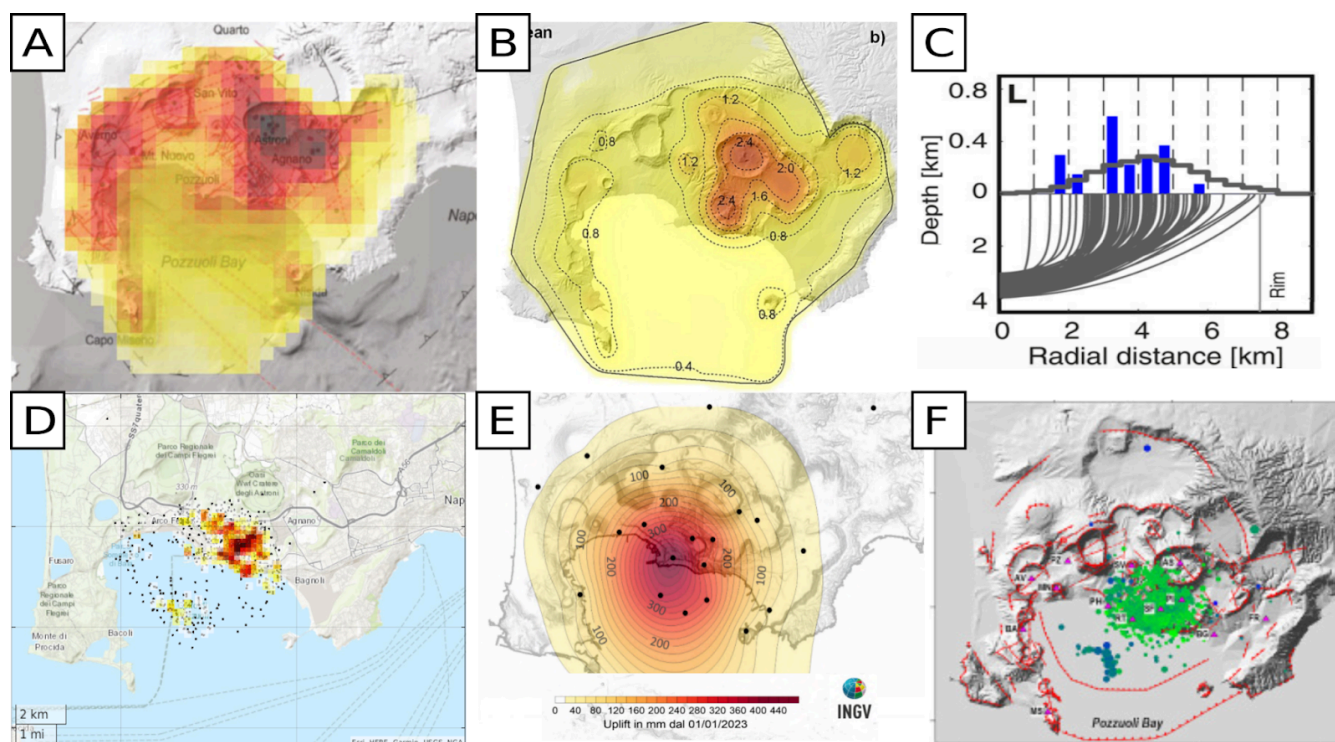
163

Figure 3: (A) Vent opening probability maps form Selva et al. (2012). (B) Vent opening probability map from Bevilacqua et al. (2015). (C) Forecasted distances from the center of the caldera from Rivalta et al. (2019) (D) Spatial density of Campi Flegrei seismicity (Md > 1) in the period June 2023 - June 2025. (E) uplift in the period January 2023 - June 2025 (modified from Osservatorio Vesuviano 2025). (F) 2011–2022 seismicity (green circles) and main structural features (magenta lines): outcropping faults, the Campanian Ignimbrite and Neapolitan Yellow Tuff caldera borders and outer/inner rims (modified from Tizzani et al 2024).

170 Also the probability peak at Solfatara, which is found in both maps produced here, is more evident here than in literature
171 studies. This is a consequence of combining the peaks in distance and angles. This effect is also evident in the other
172 secondary probability peaks at sea in the E and SE directions, in the direction of the topographic peaks of Baia and Capo
173 Miseno. These peaks emerge here, but they were not found in literature studies, and they essentially coincide with one spot
174 of high seismic activity recorded in the ongoing unrest episode (Fig. 3D), as well as in the past monitored unrest episodes. In
175 particular, in Fig. 3D, we report the spatial density of the seismicity recorded in the last two years, which shows a striking
176 correspondence to the vent probability maps reported in Fig. 2A.

7

177 More in general, the two higher probability rings that emerge here correspond to the position of the ring faults surrounding
178 the inner caldera and bordering the area of maximum uplift (Fig 3D and 3F, Tizzani et al. 2024, Natale et al. 2025). These
179 observations are completely independent and may help spotting privileged paths for magma ascent around the NYT caldera
180 border.

Datasets

182 The position of the vents related to past eruptions was obtained from Bevilacqua et al. (2015). The DEM of the area obtained
183 from TINITALY (Tarquini et al. 2023) with WGS 84 / UTM zone 33N coordinates, available at https://tinitaly.pi.ingv.it/.

Acknowledgements

185 The figures and maps have been produced using Matlab and/or InkScape software.

References

187 Alberico, I., Lirer, L., Petrosino, P., & Scandone, R. (2002). A methodology for the evaluation of long-term volcanic risk
188 from pyroclastic flows in Campi Flegrei (Italy). Journal of Volcanology and Geothermal Research, 116, 63–78.
189 https://doi.org/10.1016/S0377-0273(02)00211-1

191 Amoruso, A., Crescentini, L., Sabbetta, I., De Martino, P., Obrizzo, F., & Tammaro, U. (2014). Clues to the cause of the
192 2011–2013 Campi Flegrei caldera unrest, Italy, from continuous GPS data. Geophysical Research Letters, 41, 1–7.
193 https://doi.org/10.1002/2014GL059539

195 Barberi, F., Corrado, G., Innocenti, F., & Luongo, G. (1984). Phlegraean fields 1982–1984: Brief chronicle of a volcano
196 emergency in a densely populated area. Bulletin of Volcanology, 47, 175–185. https://doi.org/10.1007/BF01961547

198 Bevilacqua, A., Isaia, R., Neri, A., Vitale, S., Aspinali, W. P., Bisson, M., Flandoli, F., Baxter, P. J., Bertagnini, A., Ongaro,
199 T. E., Iannuzzi, E., Pistolesi, M., & Rosi, M. (2015). Quantifying volcanic hazard at Campi Flegrei caldera (Italy) with
200 uncertainty assessment: 1. Vent opening maps. Journal of Geophysical Research: Solid Earth, 120, 2309–2329.
201 https://doi.org/10.1002/2014JB011775

8

203 Bevilacqua, A., Neri, A., De Martino, P. et al. (2024). Accelerating upper crustal deformation and seismicity of Campi
204 Flegrei caldera (Italy), during the 2000–2023 unrest. Commun Earth Environ 5, 742.
205 https://doi.org/10.1038/s43247-024-01865-y

207 Buono, G., Paonita, A., Pappalardo, L., Caliro, S., Tramelli, A., & Chiodini, G. (2022). New insights into the recent magma
208 dynamics under Campi Flegrei caldera (Italy) from petrological and geochemical evidence. Journal of Geophysical
209 Research: Solid Earth, 127, e2021JB023773. https://doi.org/10.1029/2021JB023773

211 Charlton, D., Kilburn, C., & Edwards, S. (2020). Volcanic unrest scenarios and impact assessment at Campi Flegrei caldera,
212 Southern Italy. Journal of Applied Volcanology, 9(7). https://doi.org/10.1186/s13617-020-00097-x

214 Chiodini, G., et al. (2021). Hydrothermal pressure–temperature control on CO_2 emissions and seismicity at Campi Flegrei
215 (Italy). Journal of Volcanology and Geothermal Research, 414, 107245. https://doi.org/10.1016/j.jvolgeores.2021.107245

217 D'Antonio, M., Tonarini, S., Arienzo, I., Civetta, L., & Di Renzo, V. (2007). Components and processes in the magma
218 genesis of the Phlegrean Volcanic District (Southern Italy). In L. Beccaluva, G. Bianchini, & M. Wilson (Eds.), Cenozoic
219 volcanism in the Mediterranean area (pp. 203–220). Geological Society of America Special Paper 418.

221 Del Gaudio, C., Aquino, I., Ricciardi, G. P., Ricco, C., & Scandone, R. (2010). Unrest episodes at Campi Flegrei: A
222 reconstruction of vertical ground movements during 1905–2009. Journal of Volcanology and Geothermal Research, 195,
223 48–56. https://doi.org/10.1016/j.jvolgeores.2010.02.002

225 Di Vito, M. A., Isaia, R., Orsi, G., Southon, J., de Vita, S., D'Antonio, M., Pappalardo, L., & Piochi, M. (1999). Volcanism
226 and deformation since 12,000 years at the Campi Flegrei caldera (Italy). Journal of Volcanology and Geothermal Research,
227 91(2–4), 221–246. https://doi.org/10.1016/S0377-0273(99)00037-2

229 Giudicepietro, F., Avino, R., Bellucci Sessa, E., et al. (2025). Burst-like swarms in the Campi Flegrei caldera accelerating
230 unrest from 2021 to 2024. Nature Communications, 16, 1548. https://doi.org/10.1038/s41467-025-56723-y

232 Isaia, R., Marianelli, P., & Sbrana, A. (2009). Caldera unrest prior to intense volcanism in Campi Flegrei (Italy) at 4.0 ka
233 B.P.: Implications for caldera dynamics and future eruptive scenarios. Geophysical Research Letters, 36, L06304.
234 https://doi.org/10.1029/2008GL036962

236 Orsi, G., Di Vito, M. A., & Isaia, R. (2004). Volcanic hazard assessment at the restless Campi Flegrei caldera. Bulletin of
237 Volcanology, 66, 514–530. https://doi.org/10.1007/s00445-003-0327-4

239 Osservatorio Vesuviano (2025), Bollettino di Sorveglianza CAMPI FLEGREI GIUGNO 2025 A cura della Sezione di
240 Napoli, available at
241 https://www.ov.ingv.it/index.php/monitoraggio-e-infrastrutture/bollettini-tutti/bollett-mensili-cf/anno-2025-3/1850-bollettino
242 -mensile-campi-flegrei-2025-06/file

244 Rivalta, E., Corbi, F., Passarelli, L., Acocella, V., Davis, T., & Di Vito, M. A. (2019). Stress inversions to forecast magma
245 pathways and eruptive vent location. Science Advances, 5, eaau9784. https://doi.org/10.1126/sciadv.aau9784

247 Sbrana, A., Marianelli, P., & Pasquini, G. (2021). The Phlegrean Fields volcanological evolution. Journal of Maps, 17(2),
248 557–570. https://doi.org/10.1080/17445647.2021.1982033

250 Selva, J., Orsi, G., Di Vito, M. A., Marzocchi, W., & Sandri, L. (2012). Probability hazard map for future vent opening at the
251 Campi Flegrei caldera, Italy. Bulletin of Volcanology, 74, 497–510. https://doi.org/10.1007/s00445-011-0528-2

253 Smith, V. C., Isaia, R., & Pearce, N. J. G. (2011). Tephrostratigraphy and glass compositions of post–15 kyr Campi Flegrei
254 eruptions: Implications for eruption history and chronostratigraphic markers. Quaternary Science Reviews, 30, 3638–3660.
255 https://doi.org/10.1016/j.quascirev.2011.08.017

257 Tarquini, S., Isola, I., Favalli, M., Battistini, A., & Dotta, G. (2023). TINITALY, a digital elevation model of Italy with a
258 10 m cell size (Version 1.1) [Data set]. Istituto Nazionale di Geofisica e Vulcanologia (INGV).
259 https://doi.org/10.13127/tinitaly/1.1

261 Tizzani, P., Fernández, J., Vitale, A., Escayo, J., Barone, A., Castaldo, R., Pepe, S., De Novellis, V., Solaro, G., Pepe, A.,
262 Tramelli, A., Hu, Z., Samsonov, S.V., Vigo, I., Tiampo, K.F., Camacho, A.G. (2024). 4D imaging of the volcano feeding
263 system beneath the urban area of the Campi Flegrei caldera, Remote Sensing of Environment, 315, 114480,
264 https://doi.org/10.1016/j.rse.2024.114480